# Aircraft Classification Based on Radar Cross Section of Long-Range Trajectories

**PIOTR PTAK**
**JUHA HARTIKKA**
**MAUNO RITOLA**
**TUOMO KAURANNE**
Lappeenranta University of Technology
Lappeenranta, Finland

**The paper studies instantaneous Doppler signature extraction from within a very high frequency (VHF) band spectrogram presented by the authors in previous work. The context of the current method is long-range aircraft detection by VHF Doppler effect. The method proposed calculates bistatic radar (BR) cross-section (BRCS) profiles and the correlation between them for different types of aircraft. The analysis is based on data represented by automatic dependent surveillance-broadcast (ADS-B) trajectory collection and passive BR with TV station as an illuminator of opportunity. Throughout the analysis, ADS-B data on location of an aircraft were adjusted with the use of extracted Doppler shift information. Then, this ground truth information on location was used for proper evaluation of BRCS profiles and, finally, for validation of the extraction method. The method is able to classify common intercontinental aircraft by size class with 70% accuracy from a 100-km distance by using an illuminator of opportunity located 300 km away.**

Manuscript received February 22, 2015; revised May 14, 2015; released for publication May 18, 2015.

DOI. No. 10.1109/TAES.2015.150139.

Refereeing of this contribution was handled by S. Watts.

Authors' addresses: P. Ptak, J. Hartikka, M. Ritola, T. Kauranne, Lappeenranta University of Technology, Mathematics and Physics, Skinnarilankatu 34, 53850 Lappeenranta, Finland, E-mail: (piotr.pawel.ptak@gmail.com).


0018-9251/15/$26.00 © 2015 IEEE

## I. INTRODUCTION

The almost 80 y long history of bistatic radar (BR) demonstrates to us that this subject resurged for a reason. With advanced technology and increasing computational power of processors, we are able to use more of the features given by BR systems. BR has been tested in a number of military applications: homing missile control, forward scatter fences, and multistatic radars.

In this and previous related work, the authors have attempted to construct a cheap and easily exploitable method for tracking aircraft in a passive bistatic configuration. The strategy of using Doppler-only information is introduced and tested in a real-life scenario in [1]. This method is further enhanced in [2] by developing a method for instantaneous Doppler extraction from within spectrogram representation of a VHF-band scattered signal. The method was tested for component detection in the spectrogram in a long-range baseline scenario (301 km), as well as with numerous statistical methods, including nonfluctuating, Swerling I and II and synthetic ogive models.

The scope of this paper is further elaboration of this extraction method. This time, the model is used for examination of BR cross-section (BRCS) profiles for classification of aircraft.

Recent publications related to the subject of BRCS include problems such as the instrument landing system misguidance of landing course aircraft by taxed large-sized aircraft [3], influence on plane electromagnetic wave reflection, and therefore BRCS, caused by radionuclide coating on the aircraft's surface with different atmospherical conditions [4].

In [5], the authors studied BRCS profiles of Panavia 200 Tornado and a Lockheed F117 Nighthawk in a terahertz time domain. The decimeter band used for both receiving and transmitting photoconductive antennas on scaled models resulted in very accurate measurements of their profiles, down to the precision of distinguishing aircraft equipped with bombs from ones without them.

In other studies [6, 7], a novel method for noncooperative target recognition based on BRCS and automatic dependent surveillance-broadcast (ADS-B) information within passive BR (PBR) configuration is developed. The authors successfully classified detected aircraft into two groups of large-size aircraft and mid-size aircraft. The BRCS is evaluated with a test set of trajectories, and then the metrics are applied to the BRCS for each cell in aspect angle-bistatic angle $\beta$ to construct a pattern for each size group for each cell.

The analysis presented in the current work differs from the aforementioned contributions. First, it uses PBR of very high frequency (VHF) band in a long-distance tracking for about 330 km of the aircraft's trajectory length. Second, the method of extracting Doppler signature is independently evaluated aside from the ADS-B-based synthetic Doppler prior information that suggests the approximate location of Doppler shift on the

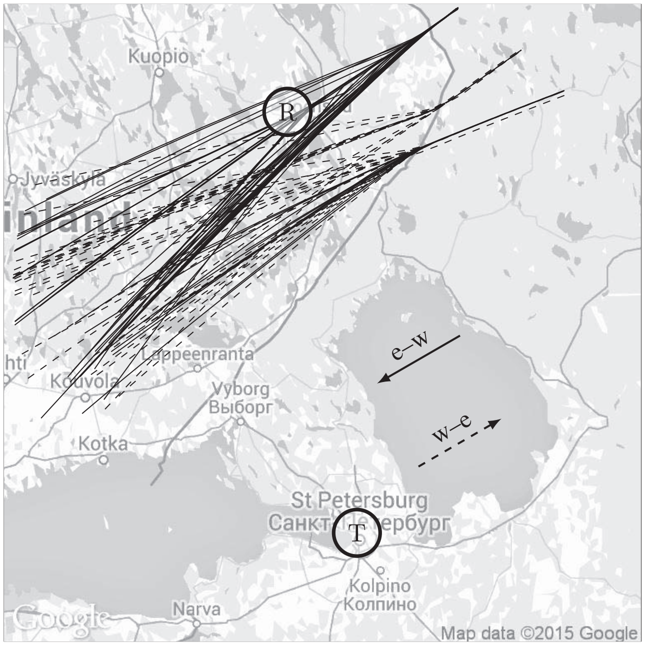


Fig. 1. Geographical location of transmitter T, receiver R, and trajectories of FR24 data. Solid and dashed lines correspond to e-w and w-e azimuths, respectively.

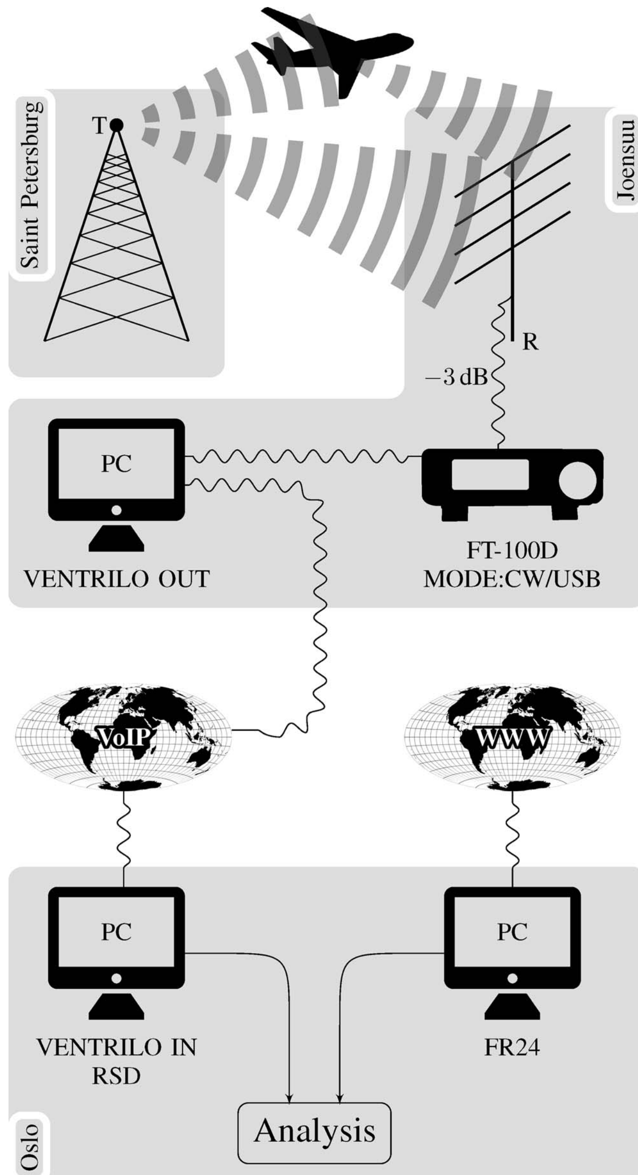


Fig. 2. Equipment (sources) used for collecting RSD and FR24.

time-frequency plane. The approach presented here differs from [6] also because we use the proximity of trajectories as a grouping factor rather than aspect angle-bistatic angle sectioning.

## II. DATA ACQUISITION AND PREPROCESSING

This section describes the configuration of PBR used and preparation of the recorded data for further analysis.

### A. Acquisition

Radio signal data (RSD) used for the analysis were retrieved by using a four-element horizontal dipole array at about 14 m aboveground and a gain of 4 to 5 dB. It is almost omnidirectional, except for the dipole ends, which are intentionally directed towards the chosen TV transmitter to attenuate about 20 dB of both the TV carrier and the high peak level of signal scattered from aircraft during the moment of its carrier crossing. The receiver is denoted with R in Fig. 1.

The Saint Petersburg transmitter, denoted as T in Fig. 1, has a transmitting frequency $f_t = 49.75$ MHz and effective radiated power of 149 kW. The receiver was located a distance of $d_{\mathrm{TR}} = 301.8$ km away from the transmitter. The receiving aerial is connected to a FT-100D receiver used in continuous wave/universal serial bus (CW/USB) mode with a 500-Hz filter. The coaxial feed line loss between the aerial and receiver is about 3 dB. Audio from the receiver is connected to the computer's sound card for numerical analysis. The required audio width for aircraft scatter Doppler observations is less than $\pm 100$ Hz from the 600-Hz center audio frequency. Because the audio center frequency is low and the bandwidth is very narrow, the 8-bit signal quality used for analysis is adequate.

This preprocessed signal was then sent via voice over Internet protocol with the use of Ventrilo software with a sampling frequency of 8 kHz to location in Oslo, Norway. The average signal delay varied at around 79 ms. A diagram of the RSD and Flightradar 24 (FR24) acquisition path is demonstrated in Fig. 2. The signal was then transformed using short-time Fourier transform (STFT), with an adjusted width of a symmetrically positioned Hann window of 1 s and calculation time step of 0.5 s. This overlapped form of the spectrogram guarantees that the signal's magnitude will be preserved [8]. Moreover, in [2], the authors stated that studies on first-order derivative of Doppler shift ensure the choice of the window length being correctly adjusted.

In parallel, other FR24 data were collected from the flightradar24.com Web site. The Web site uses an ADS-B

TABLE I
Types of Aircraft Together with ICAO Designator and Number of Appearances Grouped by Azimuth and Basic Specifications

| Aircraft | ICAO | Number of Trajectories e-w | Number of Trajectories w-e | Wing Area ($m^2$) | Number of Engines |
|---|---|---|---|---|---|
| • Airbus A330-300 | A333 | 9 | 7 | 363.1 | 2 |
| • Airbus A340-300 | A343 | 13 | 2 | 363.1 | 4 |
| • Airbus A340-600 | A346 | 4 | 1 | 437 | 4 |
| Boeing 737-800 | B738 | 1 | 1 | 125 | 2 |
| • Boeing 747-400 | B744 | 7 | 5 | 541.2 | 4 |
| • Boeing 777-200 | B772 | 12 | 7 | 427.8 | 2 |
| Boeing 777-200LR | B77L | 0 | 4 | 427.8 | 2 |
| • Boeing 777-300ER | B77W | 16 | 5 | 427.8 | 2 |
| • Boeing 787-8 Pax2 | B788 | 3 | 1 | 325 | 2 |
| Gulfstream V | GLF5 | 1 | 0 | 105.6 | 2 |

The bullet sign indicates aircraft used in the analysis.

system as a means of collecting a data. The FR24 data consist of tracks of aircraft in proximity to the transmitter and the receiver. The tracks, on the other hand, were built of the following most relevant columns of data: latitude, longitude, altitude, aircraft type designator [International Civil Aviation Organization (ICAO)], and the wall-clock time of the sample being measured. The data/message formats for Mode S (common protocol for tracking and identifying an aircraft) specific services are defined in [9]. The sample was collected on average every 5 s. During recordings of FR24, 99 different trajectories created by 11 different types of aircraft were collected from which seven most frequent types were used for the analysis (see Table I). The trajectories are depicted in Fig. 1.

## B. Preprocessing

After the synchronous recordings of RSD and FR24 have been finished, the analysis of RSD for the tracing of Doppler and carrier signatures is started. The tracing of Doppler signature and carrier was conducted by using the technique presented by the authors in [2]. The resulting data consist of vectors of Doppler frequency $f_D^{\mathrm{RSD}}$ and the associated amplitude $A_D$ as a function of time $t$, as well as carrier frequency $f_c$ and the associated amplitude $A_c$ as a function of time $t$. For each extracted signature, the associated FR24 signature was found by calculating the proximity between the extracted Doppler and the FR24-resulted Doppler on time-frequency plane.

The FR24-related Doppler signature $f_D^{\mathrm{FR24}}$ was calculated based on the spherical coordinates $lat$, $lon$, and altitude $alt$, with respect to the location of the transmitter T and the receiver R by the following formulae (1) and (2):

$$f_D^{\mathrm{FR24}}(t) = \frac{f_t}{c}\frac{d\left(d_{\mathrm{TA}}(t) + d_{\mathrm{AR}}(t)\right)}{dt} \tag{1}$$

$$d_{\mathrm{TA(AR)}}(t) = \left[2R_E\left(R_E + alt(t)\right)\left(1 - cos\left(\xi_{\mathrm{TA(AR)}}\right)\right) + alt(t)^2\right]^{\frac{1}{2}}, \tag{2}$$

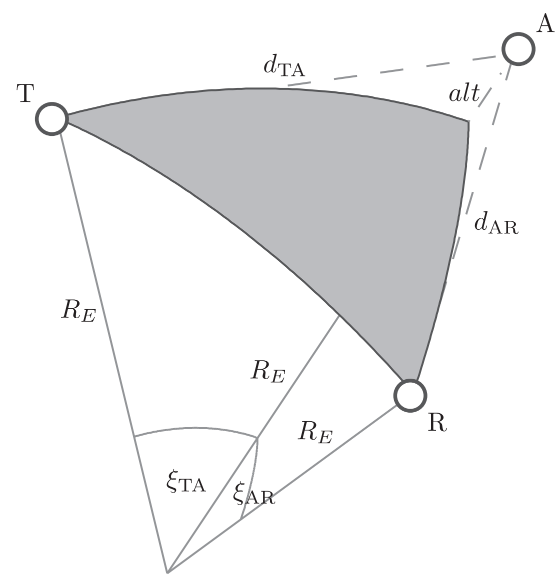


Fig. 3. Geometry used in (2).

where $R_E = 6371$ km is the mean radius of the Earth, $\xi_{\mathrm{TA}}$ and $\xi_{\mathrm{AR}}$ correspond to great circle arcs, measured in degrees and connecting the transmitter with the aircraft and the aircraft with the receiver, respectively, $c$ is the velocity of propagation of electromagnetic waves (light), $d_{\mathrm{TA}}$, $d_{\mathrm{AR}}$, and $d_{\mathrm{TR}}$ denote distances between the transmitter and an aircraft, an aircraft and receiver, and transmitter and receiver (baseline), respectively. The angles were derived with the use of Vincenty's inverse formulae [10] and based on the 1984 World Geodetic System spheroid. Clarification of these notations is presented in Fig. 3.

Because the trajectory based on the latitude and longitude information of FR24 was distorted, the resulting Doppler frequency $f_D^{\mathrm{FR24}}$ was distorted, too (see yellow dots in Fig. 4). The noisy data are due to asynchronous data collection by different ADS-B parties, caused, most likely, by differences in the clock time settings of the personal computer (PC) and partially by delay from the time when the global positioning system measurement

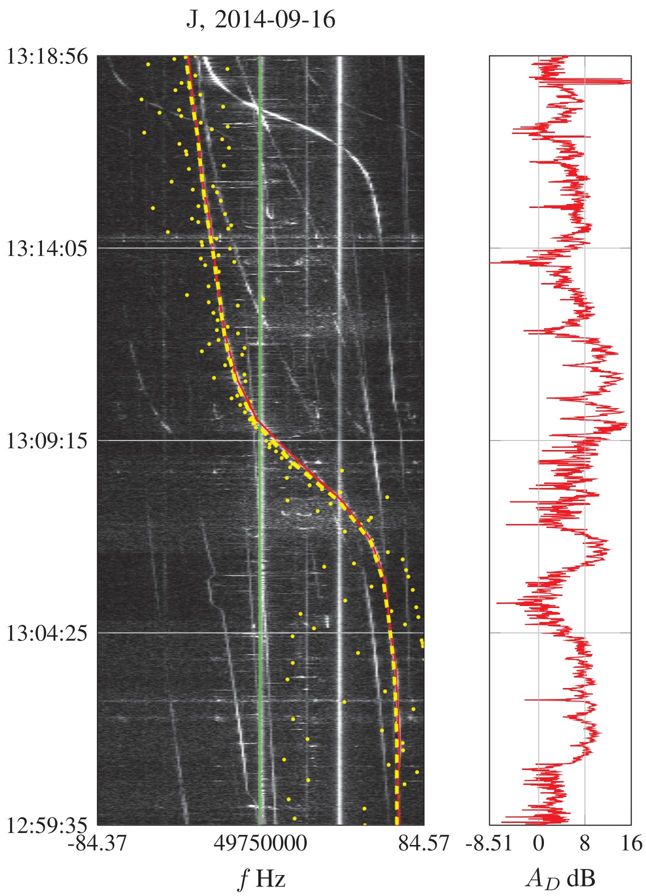


Fig. 4. Spectrogram: yellow dots—Doppler shift based on FR24 data $f_D^{\mathrm{FR24}}$; yellow dashed line—smoothed Doppler shift based on FR24 data $f_D^{\mathrm{FR24*}}$; red line—extracted Doppler curve $f_D^{\mathrm{RSD}}$; green line—extracted carrier $f_c$. Right: amplitude of extracted Doppler signature $A_D$.

was taken onboard the aircraft to the time of reception with the ADS-B receiver. In reality, the aircraft path obtained from FR24 (ADS-B) follows the right trajectory, but the location of the plane may oscillate back and forth around the correct location, which means that the aircraft's direction of movement is often opposite (180°) to the real one. These inaccuracies lead to high discontinuities on the time-frequency plane, as presented in Fig. 4. The reason why these inaccuracies have arisen is not completely clear, but one of the explanations might be the secure policy of transported goods.

To compensate for this noise, the data on latitude *lat*, longitude *lon*, and altitude *alt* was transformed from spherical to Cartesian coordinates, then smoothed and interpolated with respect to time *t*. The smoothing window was equal to 10 s, and interpolation was chosen to match the time resolution of RSD data 0.5 s. At the end, the interpolated data were transformed back to spherical coordinates, and the Doppler frequency was calculated and denoted by $f_D^{\mathrm{FR24*}}$ (see yellow dashed line in Fig. 4).

Because the information on Doppler shift $f_D^{\mathrm{RSD}}$ was extracted from within the spectrogram (see red line on the spectrogram in Fig. 4), it can now be used for further adjustment of the trajectory of an aircraft. Note that the synthetic Doppler (FR24) projected onto the spectrogram does not overlap with the extracted Doppler. There is a noticeable shift between them with respect to time, and the close-to-baseline region of the FR24 signature is steeper than that of RSD (see Fig. 4). The remedy for this difference was introduced by shifting the whole trajectory by latitude $lat_{sh}$ and longitude $lon_{sh}$ factors and looking for the minimum cost function that is presented in (3).

$$f_{cost} = |f_D^{\mathrm{FR24*}} - f_D^{\mathrm{RSD}}| \frac{f_{D,\max}}{f_{D,\max} + |f_D^{\mathrm{RSD}}|}, \tag{3}$$

where $f_{D,\max}$ denotes the maximum achievable Doppler shift, which is expressed by

$$f_{D,\max} = 2\frac{f_t}{c} V_{c,\max}. \tag{4}$$

In the case of maximum cruising velocity, $V_{c,\max}$ is set to $V_{c,\max} = 278$ m/s, which yields $f_{D,\max} = 92$ Hz. The proposed form of cost function intentionally puts higher weight onto the region close-to-baseline crossing to account for the shift in time between the signatures. The found distribution of latitude and longitude shifts in polar coordinates is presented in Fig. 5. Most of the trajectory shifts do not exceed a 5-km boundary. The curve distribution pattern in the east-west (e-w) group would suggest that the needed shift was dictated not only by time delay but also by displacement in spherical coordinates.

By this process, RSD data were now also accompanied by FR24-based information, such as trajectory (latitude *lat**, longitude *lon**, and altitude *alt*), type of an aircraft ICAO, and the FR24-based Doppler curve. This set of numbers can be denoted by $\{f_D^{\mathrm{RSD}},\ A_D,\ f_c,\ A_c,\ lat^*,\ lon^*,\ alt,\ f_D^{\mathrm{FR24*}}\},\ (t)$. This set can be further divided into two subsets, namely, those azimuth related to west-east (w-e) and e-w. All of the analyses take into account the e-w group. Additionally, the remaining group of aircraft is categorized by their size into three groups: **G1**: mid-size (B788, A333, and A343); **G2**: large-size (B772, B77W, and A346); and the largest aircraft **G3**: (B744).

## III. RADAR CROSS-SECTION COMPARISON

The BRCS $\sigma_B$ of the extracted signatures was calculated by using the following [11]:

$$\sigma_B = \frac{A_D}{A_c} = \frac{(4\pi)^3 d_{\mathrm{TA}}^2 d_{\mathrm{AR}}^2}{d_{\mathrm{TR}}^2}. \tag{5}$$

Equation (5) was derived from BR formulae [12] in (6)

$$A_D = \frac{P_{\mathrm{T}} G_{\mathrm{T}} G_{\mathrm{R}} \lambda^2 \sigma_B}{(4\pi)^3 d_{\mathrm{TA}}^2 d_{\mathrm{AR}}^2} \tag{6}$$

and direct-path link budget (7) for the receiver not being in line-of-sight from the transmitter

$$A_c = P_{\mathrm{T}} G_{\mathrm{T}} G_{\mathrm{R}} L_S, \tag{7}$$

where $P_{\mathrm{T}}$ is the transmitter power output, $G_{\mathrm{T}}$ is the transmitting antenna power gain, $G_{\mathrm{R}}$ is the receiving

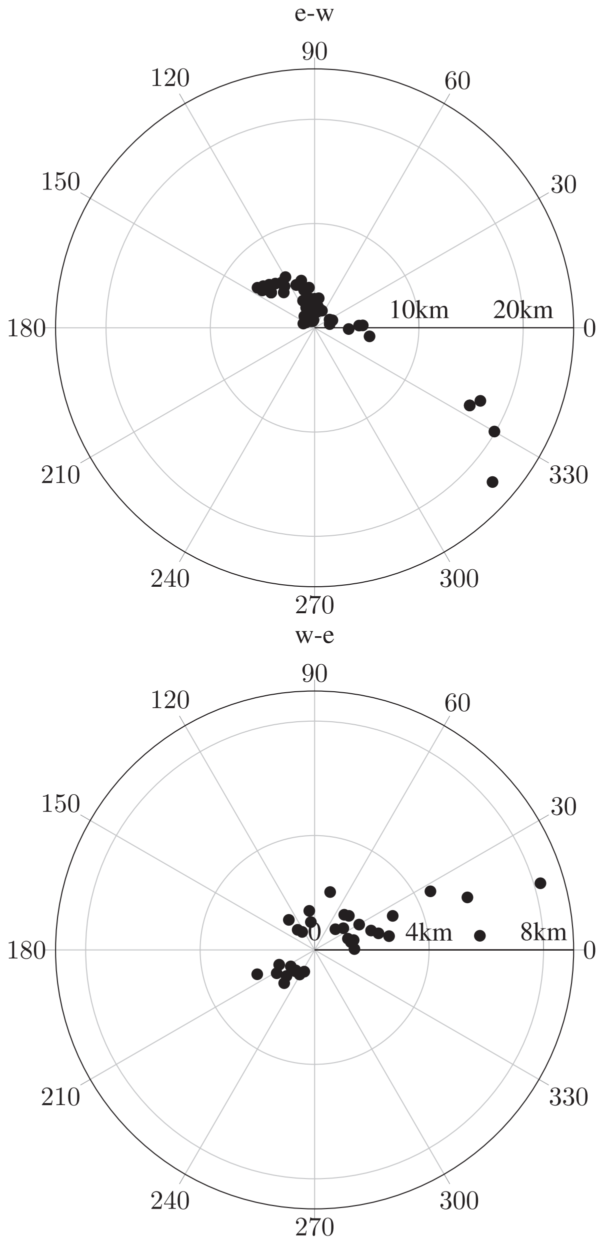

Fig. 5. Distribution of found latitude and longitude shifts $lat_{sh}$, $lon_{sh}$ (azimuth, distance kilometers) for groups e-w (top) and w-e (bottom).

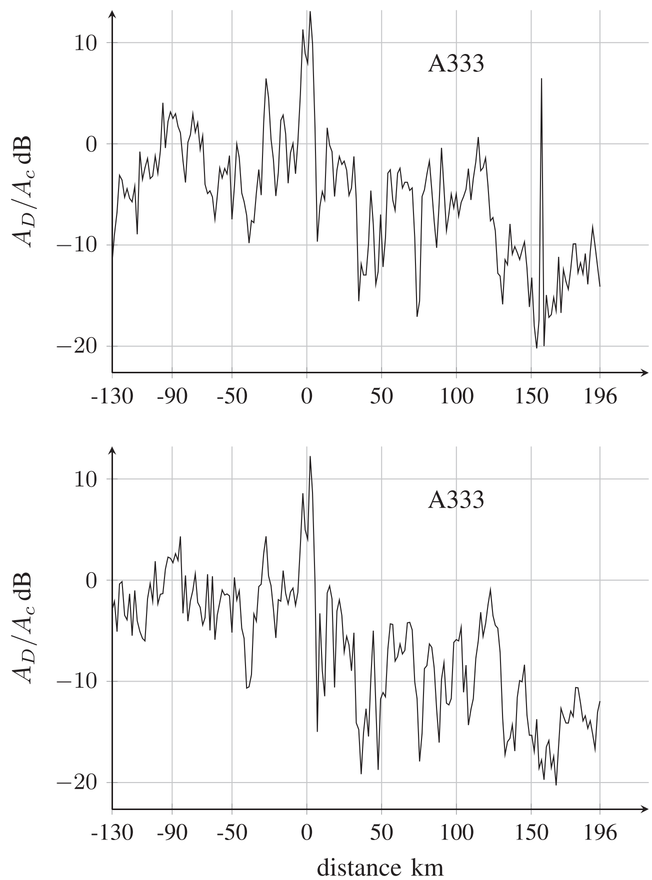

Fig. 6. Fraction of reflected to direct signal from two Airbus A330-300 aircrafts in time domain.

TABLE II
An Average Correlation with Respect to the Type of an Aircraft

| ICAO | B788 | A333 | A343 | B772 | B77W | A346 | B744 |
|---|---|---|---|---|---|---|---|
| B788 | 0.57 | 0.65 | 0.56 | 0.28 | 0.20 | 0.28 | 0.20 |
| A333 | 0.65 | 0.74 | 0.65 | 0.31 | 0.35 | 0.41 | 0.24 |
| A343 | 0.56 | 0.65 | 0.70 | 0.36 | 0.42 | 0.34 | 0.29 |
| B772 | 0.28 | 0.31 | 0.36 | 0.75 | 0.73 | 0.69 | 0.35 |
| B77W | 0.20 | 0.35 | 0.42 | 0.73 | 0.76 | 0.71 | 0.36 |
| A346 | 0.28 | 0.41 | 0.34 | 0.69 | 0.71 | 0.80 | 0.38 |
| B744 | 0.20 | 0.24 | 0.29 | 0.35 | 0.36 | 0.38 | 0.75 |

antenna power gain, $\lambda$ is the wavelength, and $L_S$ denotes free-space path loss of the signal between the transmitter and the receiver. No other losses are assumed. The free-space loss factor $L_S$ is expressed as

$$L_S = \left(\frac{\lambda}{4\pi d_{\mathrm{TR}}}\right)^2 \tag{8}$$

Therefore, by substituting $L_S$ from (8) into (7), then dividing sidewise (7) and (6), and by rearranging, the form in (5) is attained. The bistatic angle $\beta$ is estimated from the location of the aircraft, the transmitter, and the receiver to represent the BRCS as a function of $\beta$.

Because the observed aircrafts' trajectories were not overlapping each other (more than one air corridor was used), the subsequent analysis have been carried out under a trajectory proximity assumption. The validity of this assumption is tested by analyzing trajectories pairwise, taking into account the average horizontal distance between them that should be relatively small. In the case in which trajectories are located in the immediate neighborhood of the receiver, the propagation of the bounced signal is no longer classified as a two-dimensional case, but as a three dimensional one, and proximity is judged accordingly. An average distance between two trajectories $tr_i$ and $tr_j$ is derived by taking every point of these two sequences

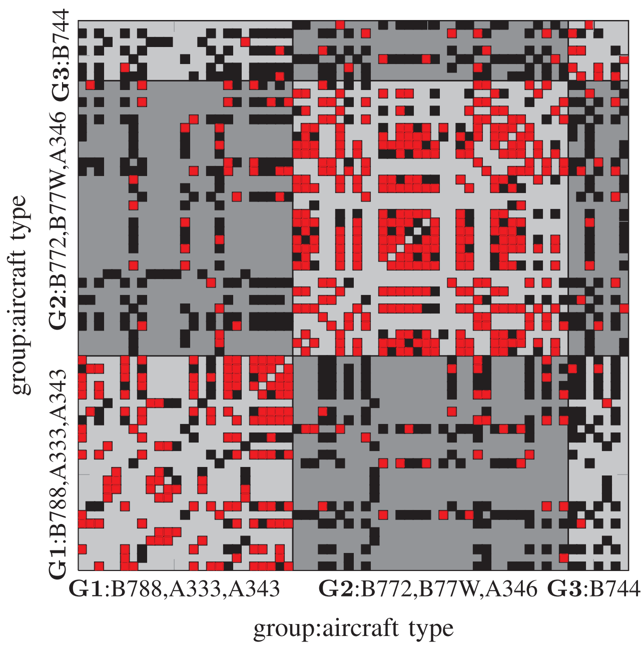


Fig. 7. Result of optimal correlation-threshold estimation. Red squares denote values over threshold, and black ones indicate values below threshold.

$tr_i(k) = (lat_i^*(k), lon_i^*(k)), k = 1, \ldots, n, tr_j(l) = (lat_j^*(l), lon_j^*(l)), l = 1, \ldots, m$ and solving (9).

$$d\left(tr_i, tr_j\right) = 0.5\left[\frac{1}{m}\sum_{l=1}^{m}\min_{k\in[1,n]} d\left(tr_i(k), tr_j(l)\right) + \frac{1}{n}\sum_{k=1}^{n}\min_{l\in[1,m]} d\left(lr_i(k), tr_j(l)\right)\right], \quad (9)$$

where $d(tr_i(k), tr_j(l))$ is a distance between $tr_i(k)$ and $tr_j(l)$. Flight trajectory pairs were screened for an arbitrarily chosen maximal minimum distance $d_{\min} = 10$ km that had to be attained between the trajectories. This screening resulted in 618 pairs of trajectories being selected for further analysis out of the 2145 available at the beginning.

Fig. 6 depicts a fraction of the difference in amplitude of the extracted Doppler signal and the extracted carrier signal for two aircraft of type A333 in the distance domain. The distance domain describes the distance from an aircraft to the baseline, negative for the approaching part and positive for the departing part. In this example, a correlation between signals reached $\rho = 0.92$, while the average distance between trajectories equaled $d\,(tr_i, tr_j) = 0.52$ km.

As mentioned earlier, the performance of the technique presented in [2] ought to be tested by checking the correlation between calculated BRCSs for different types of aircraft. This is achieved by calculating the correlation between BRCS for every pair of trajectories available, then classifying them by the aircraft type, and finally calculating an average correlation factor. The result of this analysis is presented in Table II.

We notice the relatively higher correlation factors of the three groups on the diagonal of the matrix. In the next analysis, we have found an optimal correlation threshold for which the number of aircraft pairs from the same class is maximized and the pairs from different classes is minimized. The threshold has been found to be equal $\rho_t = 0.58$. The result for this is shown in Fig. 7. The detailed description of the procedure of estimating an optimal threshold is presented in Fig. 8. The estimation is represented here by use of two FOR loops, one inside another. The inner loop checks all the combinations of trajectories $tr_i$ and $tr_j$ for the system of IF rules, which

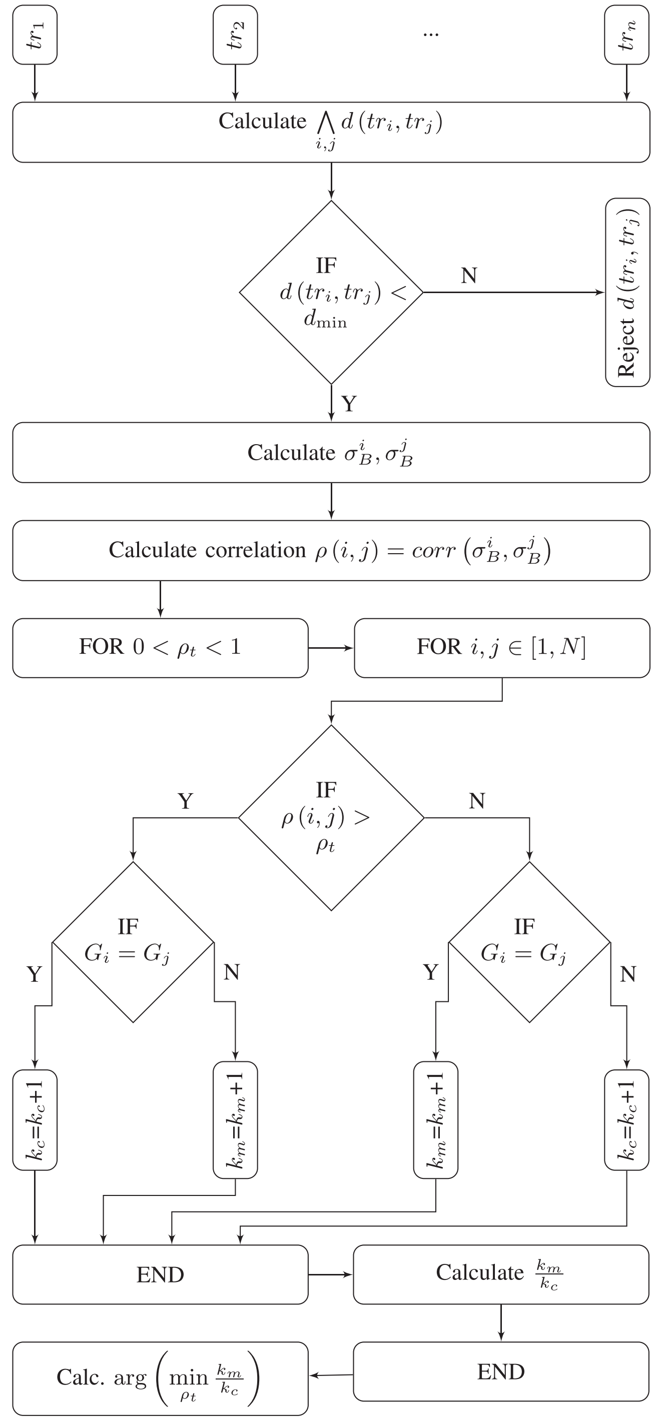


Fig. 8. Procedure of estimating optimal correlation threshold whose effects are presented in Fig. 7.

TABLE III
Probability of Classification/Misclassification Between Groups G1, G2, and G3

| | Aircraft Group | | |
|---|---|---|---|
| | G1: B788, A333, A343 | G2: B772, B77W, A346 | G3: B744 |
| G1 | $\frac{74}{101} = \mathbf{0.73}$ | $\frac{34}{171} = 0.19$ | $\frac{4}{59} = 0.06$ |
| G2 | $\frac{34}{171} = 0.19$ | $\frac{162}{205} = \mathbf{0.79}$ | $\frac{12}{75} = 0.16$ |
| G3 | $\frac{4}{59} = 0.06$ | $\frac{12}{75} = 0.16$ | $\frac{5}{7} = \mathbf{0.71}$ |

examine the quality of misclassification to classification ratio $\frac{k_m}{k_c}$. The IF rule $G_i = G_j$ checks if trajectories $i$ and $j$ represent the same aircraft size group. The outer loop checks for all values of $\rho_t$ that satisfies $0 < \rho_t < 1$.

The number of correctly classified pairs within groups on the diagonal significantly exceed the number of misclassified pairs. With this condition in mind, the probability of misdetection/detection was calculated and presented in Table III. The values on the diagonal reflect the probability of correct classification, whereas the upper and lower triangles indicate the probability of misclassification.

## IV. DISCUSSION

The paper validates the performance of the mathematical model of instantaneous Doppler signature extraction from within the VHF band spectrogram image [2] by comparing the BRCS profiles of seven types of aircraft. First, the FR24 and RSD data were acquired, from which the latter was preprocessed by using STFT. Then, with the technique presented in [2], Doppler and carrier signatures were estimated. In parallel, the FR24 data were enhanced by smoothing and interpolating trajectories to denoise the data. Additionally, with the use of the extracted Doppler shift information, the FR24 trajectories were shifted to minimize the frequency distance between FR24 and RSD Doppler shifts. Then, the BRCS for each Doppler amplitude $A_D$ and associated carrier amplitude $A_c$ and trajectory (*lat**, *lon**) was calculated. Because of different air corridors used by recorded aircraft, further analysis of BRCS comparison was conducted, with respect to the distance between trajectories. The correlation between BRCSs was calculated for each pair of trajectories for which the average distance does not exceed 10 km. The resulting matrix of correlations, especially diagonal values, between different types of the aircraft validates the extraction technique, as well as the data acquisition and preprocessing methods, as does the further examination of classification performance by means of thresholding the correlation to estimate the optimal classification to misclassification ratio.

## REFERENCES


[1] Ptak, P., Hartikka, J., Ritola, M., and Kauranne, T.
Long-distance multistatic aircraft tracking with VHF frequency Doppler effect.
*IEEE Transactions on Aerospace and Electronic Systems*, **50**, 3 (July 2014), 2242–2252.

[2] Ptak, P., Hartikka, J., Ritola, M., and Kauranne, T.
Instantaneous Doppler signature extraction from within a spectrogram image of a VHF band.
*IEEE Transactions on Aerospace and Electronic Systems.* Accepted to be published in **52**, 2, April 2016.

[3] Geise, R., Enders, A., Vahle, H., and Spieker, H.
Scaled measurements of instrument-landing-system disturbances due to large taxiing aircraft.
*IEEE Transactions on Electromagnetic Compatibility*, **50**, 3 (Aug. 2008), 485–490.

[4] Liu, W., Zhu, J., Cui, C., Wang, X., Zhang, S., Zhang, R., Tang, T., Huang, Y., and Huang, R.
The influence of plasma induced by *alpha*-particles on the radar echoes.
*IEEE Transactions on Plasma Science*, **43**, 1 (Jan. 2015), 405–413.

[5] Gente, R., Jansen, C., Geise, R., Peters, O., Gente, M., Krumbholz, N., Moller, C., Busch, S., and Koch, M.
Scaled bistatic radar cross section measurements of aircraft with a fiber-coupled THz time-domain spectrometer.
*IEEE Transactions on Terahertz Science and Technology*, **2**, 4 (July 2012), 424–431.

[6] Pisane, J., Azarian, S., Lesturgie, M., and Verly, J.
Automatic target recognition for passive radar.
*IEEE Transactions on Aerospace and Electronic Systems*, **50**, 1 (Jan. 2014), 371–392.

[7] Pisane, J.
Automatic target recognition using passive bistatic radar signals.
Ph.D. dissertation, University of Liège and École supérieure d'électricité (Supélec), Belgium, 2013.

[8] Izraelevitz, D.
Some results on the time-frequency sampling of the short-time Fourier transform magnitude.
*IEEE Transactions on Acoustics, Speech and Signal Processing*, **33**, 6 (Dec. 1985), 1611–1613.

[9] International Civil Aviation Organization.
*Technical Provisions for Mode S Services and Extended Squitter* (1st ed.). Montréal, Canada: International Civil Aviation Organization, 2008.

[10] Vincenty, T.
Direct and inverse solutions of geodesics on the ellipsoid with application of nested equations.
*Survey Review*, **22**, 176 (1975), 88–93.

[11] Proakis, J., and Salehi, M.
*Digital Communications* (5th ed.). New York: McGraw-Hill Education, 2007. Available: http://books.google.fi/books?id=HroiQAAACAAJ.

[12] Willis, N. J.
*Bistatic Radar* (2nd ed.). Raleigh, NC: SciTech Publishing, 2005. Available: http://amazon.com/o/ASIN/1891121456/.

**Piotr Ptak** received his M.Sc. degree in applied mathematics from University of Zielona Góra, Poland, in 2004 and a second M.Sc. degree in information technology from Lappeenranta University of Technology, Finland, in 2006. He has been involved in a number of different research and editorial projects ever since. He received his Ph.D. degree from Lappeenranta University of Technology in 2015. Since 2007, he has been the coeditor of the *Journal of European Consortium for Mathematics in Industry*. His research interests include tracking of airborne objects, Doppler-only tracking systems, analysis and forecast of spot market prices, and inverse problems.

**Juha Hartikka** received his M.Sc. degree in mechanical engineering from Lappeenranta University of Technology, Finland, in 1986. His interests include research in the field of wave propagation in the electrosphere, prediction of time span for introduction and utilization of new technologies, and aircraft radio scatter. Among his experiments for Quantuum Electric Ltd., one can find capacitive motor experiments that led to finding an explanation for the operation of capacitive insulator-type electrostatic motors, by means of the capacitive effect of surface charge voltage and electrostatic force amplification.

**Mauno Ritola** has had radio reception as his hobby for over 40 y. He has studied radio communication and broadcasting in Leningrad Institute of Radiocommunication and Broadcasting, Russian Federation in 1979–1981 and received the M.Sc. (B.A.) degree for economic geography from the Turku School of Economics and Business Administration, Finland, in 1990. For the last 10 y, he has worked in monitoring for reception and frequency planning for the International Broadcasting Bureau and has been a coeditor for the *World Radio TV Handbook*.

**Tuomo Kauranne** is the founder and president of Arbonaut Ltd. since 1994. He is also an associate professor in applied mathematics at Lappeenranta University of Technology. Arbonaut is a technology company based in Joensuu, Finland, which conducts forest resource mapping via remote sensing methods on six continents and integrates geographical information systems for forest sector organizations.
Dr. Kaurannes research interests include airborne and spaceborne remote sensing and mathematical modeling of geophysical, ecological, and economic processes.